4778 *Chem. Mater.* **2009,** *21,* 4778–4783
DOI:10.1021/cm900373u

CHEMISTRY OF MATERIALS
Article

Lithium Insertion and Transport in the TiO_2−B Anode Material: A Computational Study

Corinne Arrouvel, Stephen C. Parker, and M. Saiful Islam*

Department of Chemistry, University of Bath, Bath BA2 7AY, United Kingdom

Received February 9, 2009. Revised Manuscript Received September 11, 2009

TiO_2−B is a highly promising anode material for rechargeable lithium batteries. Computational studies based on density functional theory (DFT) have been carried out on this material focusing on key issues relating to lithium insertion sites and lithium diffusion paths. Our simulation model shows good reproduction of the observed crystal structure of TiO_2−B. Electronic structure calculations suggest that the lowest energy lithium site is a slightly off-center position in the *b*-axis channel for low lithium concentration ($x < 0.125$ for Li_xTiO_2−B). Our calculated cell voltages are compatible with values from electrochemical measurements. Low Li migration energies are found for pathways along the *b*-axis channel and the [001] *c*-axis direction, suggesting significant Li ion mobility in this anode material.

1. Introduction

The search for alternative materials for rechargeable lithium batteries has generated considerable research activity,[1−3] particularly for portable electronics and large-scale applications such as hybrid electric vehicles. With the conventional graphite anodes, the lithium intercalation potential is close to that of lithium plating, leading to limited inherent overcharge protection. In addition, there is an increasing contribution from solid electrolyte interface (SEI) layer formation with smaller graphite particle size.

In this context, titanium-based oxides such as TiO_2−B have become promising candidate anode materials exhibiting favorable electrochemical properties.[4−10] TiO_2−B has a high theoretical capacity (335 mAh/g) and is viewed as a superior lithium intercalation host[9] compared to the higher density rutile, anatase, and brookite polymorphs of titania.

In evaluating the influence of insertion processes on the structural and transport properties of the TiO_2−B host material, it is important to know the precise location of the lithium ion. Such information can be difficult to extract from X-ray diffraction experiments because of the weak X-ray scattering power of the light lithium ions within the host. Similarly, the migration path and activation barrier controlling lithium ion diffusion in TiO_2−B are not well established, but are crucial for a complete understanding of the electrochemical behavior of this anode material. For example, higher rate (power) capability of rechargeable lithium batteries requires facile intrinsic Li diffusion into and out of the electrode materials. To date, there are a few theoretical studies on TiO_2−B[11−13] and it has been suggested that the Li 5-fold sites in $Li_{0.75}TiO_2$−B are similar to those in $Li_2FeV_3O_8$.[14] Recently, Panduwinata and Gale[12] calculate that lithium is bound most favorably at a position close to the titania octahedral layer.

The present study uses advanced computational techniques based on density functional theory (DFT) to investigate, at the atomic level, the key issues of lithium insertion sites and diffusion pathways in the TiO_2−B system. Such DFT techniques have been applied successfully to analogous studies of other TiO_2 polymorphs[15−17]

*Corresponding author. E-mail:: m.s.islam@bath.ac.uk.

(1) Armand, M.; Tarascon, J.-M. *Nature* **2008**, *451*, 652.
(2) Whittingham, M. S. *Dalton Trans.* **2008**, *40*, 5424.
(3) Palacin, R. *Chem. Soc. Rev.* **2009**, *38*, 2565.
(4) Armstrong, A. R.; Armstrong, G.; Canales, J.; Garcia, R.; Bruce, P. G. *Adv. Mater.* **2005**, *17*, 862. Armstrong, G.; Armstrong, A. R.; Canales, J.; Bruce, P. G. *Electrochem. Solid-State Lett.* **2006**, *9*, A139.
(5) Zukalová, M.; Kalbác, M.; Kavan, L.; Exnar, I.; Graetzel, M. *Chem. Mater.* **2005**, *17*, 1248. Brousse, T.; Marchand, R.; Taberna, P. L.; Simon, P. *J. Power Sources* **2006**, *158*, 571.
(6) Tsai, M. C.; Chang, J. C.; Sheu, H. S.; Chiu, H. T.; Lee, C. Y. *Chem. Mater.* **2009**, *21*, 499.
(7) Wang, Y. F.; Wu, M. Y.; Zhang, W. F. *Electrochim. Acta* **2008**, *53*, 7863.
(8) Wilkening, M.; Lyness, C.; Armstrong, A. R.; Bruce, P. G. *J. Phys. Chem. C* **2009**, *113*, 4741.
(9) Cava, R. J.; Murphy, D. W.; Zahurak, S. M.; Santoro, A.; Roth, R. S. *J. Solid State Chem.* **1984**, *53*, 64. Ferg, E.; Gummow, J.; de Kock, A.; Thackeray, M. M. *J. Electrochem. Soc.* **1994**, *141*, L147.
(10) Deng, D.; Kim, M. G.; Lee, J. Y.; Cho, J. *Energy Environ. Sci.* **2009**, *2*, 818. Jamnik, J.; Dominko, R.; Erjavec, B.; Remskar, M.; Pintar, A.; Gaberscek, M. *Adv. Mater.* **2009**, *21*, 2715. Yang, Z. G.; Choi, D.; Kerisit, S.; Rosso, K. M.; Wang, D. H.; Zhang, J.; Graff, G.; Liu, J. *J. Power Sources* **2009**, *192*, 588.
(11) Catlow, C. R. A.; Cormack, A. N.; Theobald, F. *Acta Crystallogr., Sect. B* **1984**, *B40*, 195.
(12) Panduwinata, D.; Gale, J. D. *J. Mater. Chem.* **2009**, *19*, 3931.
(13) Nuspl, G.; Yoshizawa, K.; Yamabe, T. *J. Mater. Chem.* **1997**, *7*, 2529.
(14) Tournoux, M.; Marchand, R.; Brohan, L. *Prog. Solid State Chem.* **1986**, *17*, 33.
(15) Koudriachova, M. V.; Harrison, N. M.; de Leeuw, S. W. *Solid State Ionics* **2003**, *157*, 35. Kuhn, A.; Diaz-Carrasco, P.; De Dompablo, M. E. A.; Garcia-Alvarado, F. *Eur. J. Inorg. Chem.* **2007**, 3375.
(16) Arrouvel, C.; Digne, M.; Breysse, M.; Toulhoat, H.; Raybaud, P. *J. Catal.* **2004**, *222*, 152.
(17) Morgan, B. J.; Watson, G. W. *Surf. Sci.* **2007**, *601*, 5034.

Published on Web 10/02/2009

and oxide materials for lithium batteries.[18−20] This study also extends our recent computational studies of lithium ion transport and surface structures of $LiFePO_4$ cathode materials.[21,22] The present simulations of the TiO_2−B bulk are an informative and necessary preliminary to more complex simulations of surface and nanotube structures.

2. Computational Techniques

Total energy calculations were performed within the framework of density functional theory (DFT) implemented in the Vienna Ab initio Simulation Package (VASP),[23] employing the generalized gradient approximation (GGA) of Perdew and Wang (PW91).[24] The eigenstates of the electron wave functions were expanded on a plane-wave basis set using pseudopotentials to describe the electron−ion interactions within the projector-augmented wave (PAW) approach.[25] Infinite lattice systems are modeled using periodic boundary conditions. For total energy calculations, we used a cutoff energy of 500 eV to ensure good convergence. The convergence criterion for the electronic self-consistent cycle was fixed at 0.1 meV per cell. A full relaxation of all atomic positions in the cell was performed until the geometric convergence criterion for the energy (1 meV/cell) was reached. The Brillouin zone was sampled according to the Monkhorst-Pack scheme,[26] using a sufficient number of symmetry unique k-points for convergence of each supercell system; namely a k-point grid up to $(4 \times 8 \times 6)$ for geometric optimisations of the $LiTi_8O_{16}$ cell ($x = 0.125$ for Li_xTiO_2−B).

An alternative approach would be to use the DFT+U method[27] where U is the on-site Coulomb parameter. The Dudarev approach is implemented in VASP in which only the difference $U - J$ (where J is the exchange parameter) is meaningful.[28] We recognize that some recent studies on Ti-based oxides have used the DFT+U approach[17,29] to treat Ti oxidation states; for example, Nolan et al.[29] used DFT+U to study self-doping of the rutile TiO_2 (110) surface. However, there are also numerous recent studies on defects in TiO_2,[30,31] and on lithium insertion in transition metal materials,[32,33] that have employed DFT-GGA methodology without the on-site U parameter.

In this study, our central aim is to investigate the relative energetics of the lithium insertion sites and transport pathways within TiO_2−B, which are highly dependent upon the structural properties (especially unit cell volume) of the host lattice. It is known that the present GGA method has a small systematic overestimation of cell volumes; the results in Table 1 show a difference between the calculated and experimental cell volumes for TiO_2−B of about 1.3%. We have also included a comparison of experimental and calculated unit cell volumes for four TiO_2 polymorphs using various DFT approaches as Supporting Information. This shows that using GGA-PW91 + U (4 eV), the discrepancy with the experimental volume increases to 2.3% for TiO_2−B. Moreover, this significant structural difference leads to an incorrect Li insertion site stability for low Li content in which the Li−O distances at the C site are much longer, making this site unfavorable, which disagrees with experimental neutron diffraction studies.

Table 1. Experimental and Calculated Structural Parameters of TiO_2−B

parameter	experiment[40]	calculated
a (Å)	12.1787	12.2875
b (Å)	3.7412	3.7746
c (Å)	6.5249	6.5832
α; β; γ (deg)	90.0; 107.054; 90.0	90.0; 107.054; 90.0
V (Å^3)	284.22	291.91
density (g/cm^3)	3.733	3.635

As detailed below, the DFT calculations with pure GGA (PW91) also result in better agreement with experimental cell voltages. These results are significant, because it is known that U is usually fitted to reproduce some experimental property, in effect adding a semiempirical component to the computations, as discussed by Nolan et al.[29] In short, our calculations on TiO_2−B based on GGA-PW91 show good agreement with experiment for the unit cell volume, the favorable Li insertion site and the cell voltages without the use of an on-site U parameter, and hence this is the approach that we employed in the present study.

The magnetic moment of the bulk lattice depends on the Li content (x) for the lithiated system Li_xTiO_2−B. For the composition $Li_{0.125}TiO_2$−B we considered the most stable magnetic state configuration. Analysis of charge was performed using the well-established Bader scheme,[34,35] in which the charge enclosed within the Bader volume is a useful approximation to the total electronic charge of an atom. We recognize that the partitioning of the charge density among individual atoms is not an absolute measure of charge, although in the current calculations, the Bader analysis provides a useful guide to changes in the nature of the electronic state.

For the Li insertion calculations, we examined the same composition, such as [Li]/[Ti] = 0.125. Increasing the size of the periodically repeating unit will not affect the Li−Li correlations at this particular concentration. Indeed, a key aspect of the calculations is that we are considering a low but nondilute concentration of a battery material. We are not examining the infinitesimal limit, which we argue is not a true lithium battery concentration, and so would miss the impact of the Li−Li correlations, which would likely contribute to the Li positions at low Li concentrations.

Previous studies of a wide variety of Li-intercalated transition metal compounds[18−20,36−38] have indicated that the average cell

(18) Morgan, D.; Van der Ven, A.; Ceder, G. *Electrochem. Solid-State Lett*. **2004**, *7*, A30.
(19) Kang, K.; Ceder, G. *Phys. Rev. B* **2006**, *74*, 094105.
(20) Islam, M. S.; Davies, R. A.; Gale, J. D. *Chem. Mater*. **2003**, *15*, 4280.
(21) Islam, M. S.; Driscoll, D. J.; Fisher, C. A. J.; Slater, P. R. *Chem. Mater*. **2005**, *17*, 5085.
(22) Fisher, C. A. J.; Islam, M. S. *J. Mater. Chem*. **2008**, *18*, 1209. Fisher, C. A. J.; Hart Prieto, V. M.; Islam, M. S. *Chem. Mater*. **2008**, *20*, 5907.
(23) Kresse, G.; Hafner, J. *Phys. Rev. B* **1994**, *49*, 14251. Kresse, G.; Furthmüller, J. *Comput. Mater. Sci*. **1996**, *6*, 15. Kresse, G.; Furthmüller, J. *Phys. Rev. B* **1996**, *54*, 11169.
(24) Perdew, J. P.; Wang, Y. *Phys. Rev. B* **1992**, *45*, 13244.
(25) Kresse, G.; Joubert, D. *Phys. Rev. B* **1999**, *59*, 1758.
(26) Monkhorst, H. J.; Pack, J. D. *Phys. Rev. B* **1976**, *13*, 5188.
(27) Anisimov, V. I.; Zaanen, J.; Andersen, O. K. *Phys. Rev. B* **1991**, *44*, 943.
(28) Dudarev, S. L.; Botton, G. A.; Savrasov, S. Y.; Humphreys, C. J.; Sutton, A. P. *Phys. Rev. B* **1998**, *57*, 1505.
(29) Nolan, M.; Elliot, S. D.; Mulley, J. S.; Bennett, R. A.; Basham, M.; Mulheran, P. *Phys. Rev. B*. **2008**, *77*, 235424.
(30) Graciani, J.; Ortega, Y.; Sanz, J. F. *Chem. Mater*. **2009**, *21*, 1431.
(31) Yang, K. S.; Dai, Y.; Huang, B. B.; Whangbo, M. H. *Chem. Mater*. **2008**, *20*, 6528.
(32) Anicete-Santos, M.; Gracia, L.; Beltran, A.; Andres, J.; Varela, J. A.; Longo, E. *Phys. Rev. B*. **2008**, *77*, 085112.
(33) Kang, K.; Morgan, D.; Ceder, G. *Phys. Rev. B*. **2009**, *79*, 014305.
(34) Henkelman, G.; Arnaldsson, A.; Jónsson, H. *Comput. Mater. Sci*. **2006**, *36*, 354.
(35) Bader, R. F. W., *Atoms in Molecules−A Quantum Theory*; Clarendon Press: Oxford, U. K., 1990.
(36) Aydinol, M. K.; Kohan, A. F.; Ceder, G.; Cho, K.; Joannopoulos, J. *Phys. Rev. B* **1997**, *56*, 1354.
(37) Braithwaite, J. S.; Catlow, C. R. A.; Harding, J. H.; Gale, J. D. *Phys. Chem. Chem. Phys*. **2001**, *3*, 4052.
(38) Gillot, F.; Monconduit, L.; Doublet, M. L. *Chem. Mater*. **2005**, *17*, 5817.

voltage can be derived using the Nernst relationship. For our system, lithium intercalation can be represented by the reaction

$$TiO_2 + xLi(metal) \rightarrow Li_xTiO_2 \quad (1)$$

The expression for the voltage can be written as follows

$$V(x) = \frac{-\Delta G}{xF} \quad (2)$$

where the free energy change (ΔG) can be approximated by the internal energy change per intercalated Li^+ (ΔE), because the vibrational and configurational entropy contributions to the cell voltage at room temperature are expected to be small as discussed by Braithwaite et al.[37] and Aydinol et al.[36] To estimate the internal energy, we calculated the energy $E(x)$ for a limited number of Li_xTiO_2 phases together with the energy of lithium metal, E(Li). The change in total energy of the system per intercalated lithium atom is given by

$$\Delta E(\overline{x}) = \frac{E(x_2) - [E(x_1) + (x_2 - x_1)E(\mathrm{Li})]}{x_2 - x_1} \quad (3)$$

where $E(x)$ is the total energy of Li_xTiO_2, $x_2 > x_1$ and $\overline{x} = (x_1 + x_2)/2$. It should be stressed that $\Delta E(\overline{x})$ leads to a predicted cell voltage that is an average value for all Li_xTiO_2 compositions between x_1 and x_2. Very small changes in composition are required to calculate ΔE accurately, but this requires the construction of extremely large supercells at considerable computational expense. Nevertheless, our main task here is to derive reliable trends as a function of lithium content for which these methods are well suited; as we have stressed before, the focus here has been low lithium contents in Li_xTiO_2−B using supercells of $LiTi_8O_{16}$, $LiTi_{16}O_{32}$, and $LiTi_{32}O_{64}$ with $x = 0.125$, 0.0625, and 0.031 respectively (see the Supporting Information for optimized structures). The energy of lithium metal, E(Li) was obtained by optimisation of body-centered cubic ($Im\bar{3}m$) Li metal with $a_0 = 3.491$ Å,[39] using a k-point mesh of $25 \times 25 \times 25$.

3. Results and Discussion

3.1. Crystal Structure and Lithium Insertion Sites. In order to probe the validity of our computational approach, structural optimisations of TiO_2−B were performed based on the bulk crystal structure observed experimentally.[40] The crystal structure of TiO_2−B is monoclinic (space group $C2/m$), and composed of edge and corner-sharing TiO_6 octahedra (shown in Figure 1). With respect to possible lithium diffusion, it is important to mention the existence of channels along the [010] direction. Following the structural optimisations, the calculated and experimental structural parameters are compared in Table 1 and show general agreement for the unit cell parameters.

We note that TiO_2−B contains two different types of Ti atoms (denoted Ti_1 and Ti_2) and three nonequivalent oxygen atoms, labeled O_{br} (bridging oxygen), O_{3f} (3-fold coordinated oxygen) and O_{4f} (4-fold coordinated oxygen). The bulk structure and calculated Bader charges are also included in Figure 1. The Ti_1 and Ti_2 charges are

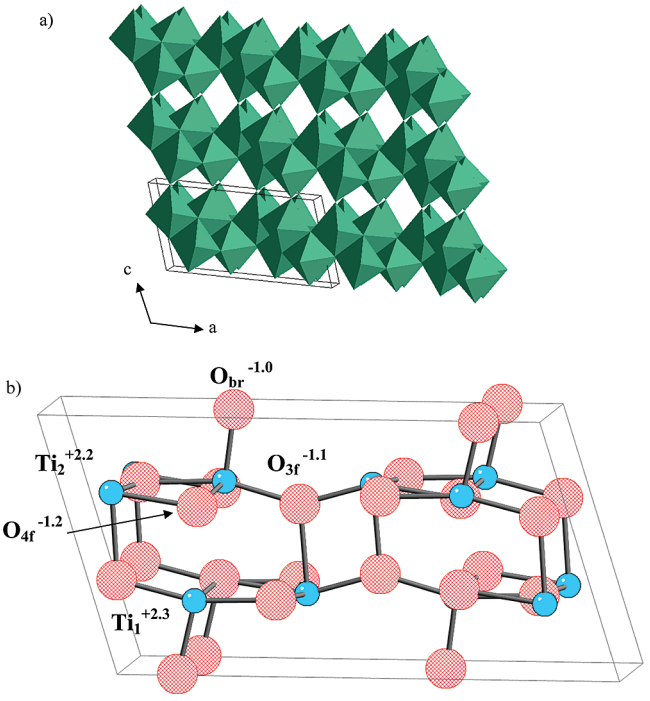

Figure 1. Bulk crystal structure of TiO_2−B: (a) ribbons of edge-sharing TiO_6 octahedra, connected in the c direction by corner-sharing; (b) ball-and-stick model of the unit cell with lattice sites and calculated Bader charges as labeled.

+2.3 and +2.2, respectively, with the O charges in the range −1.0 to −1.2. These values are different from the formal charges of +4 for Ti, and −2 for O in the fully ionic limit, and clearly indicate that the Ti−O bonds have significant covalent character. The order of the charges for oxygen is as follows $O_{4f} < O_{3f} < O_{br}$. This suggests that the bonding to the 2-fold oxygen atom (O_{br}) is the most covalent, which is also reflected by its shorter Ti−O bond lengths.

As noted, in evaluating the influence of insertion processes on the structural and transport properties of the TiO_2−B host material it is important to know the precise location of the lithium ion, which can be difficult to extract from X-ray diffraction experiments. Brohan and Marchand[41] have described possible intercalation sites in the TiO_2−B structure, labeled C, A1, and A2 (shown in Figure 2). The C site is in the middle of the cavity of the b-axis channel, and at the center of the square-planar arrangement of oxygen atoms (with Li−O distances of ~2.40 Å). The A1 site is 5-fold coordinated to oxygen within the (001) plane (with Li−O distances of 1.9−2.2 Å) and is also present in $Li_2FeV_3O_8$. The A2 site is also a 5-fold coordinated site and lies between the bridging oxygens (O_{br}) in the (001) plane (with Li−O distances of 1.9−2.1 Å).

The relative importance of these possible sites can be identified by calculating the energies for the lithium interstitial at various positions within the TiO_2−B structure (listed in Table 2). For the constant-pressure calculations, the unit-cell volume and atom positions of the host oxide were allowed to relax after lithium insertion,

(39) Barrett, C. S. *J. Phys. Chem.* **1958**, *62*, 732.
(40) Feist, T. P.; Davies, P. K. *J. Solid State Chem.* **1992**, *101*, 275.
(41) Brohan, L.; Marchand, R. *Solid State Ionics* **1983**, *9/10*, 419.

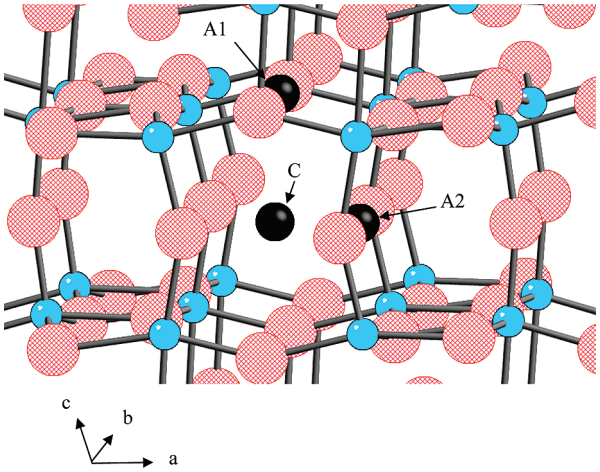

Figure 2. Possible lithium intercalation sites labeled C, A1, and A2. Large spheres are oxygen atoms (red) and small spheres are Ti atoms (blue).

Table 2. Position and Relative Energetics of Li Intercalation Sites in $Li_{0.125}TiO_2$−B

			E (eV)[a]	
Li site	initial coordinates	Wyckoff notation	constant volume	constant pressure
C	0.0 0.5 0.0	2b	0.0	0.0
A1	0.95 0.50 0.62	4i	0.11	0.15
A2	0.13 0.50 0.00	4i	0.05	0.09

[a] relative to C site.

whereas for the constant-volume calculations, only the atom positions were allowed to relax.

The relative energies in Table 2 suggest that the C site is most favorable for Li insertion at $x \leq 0.125$, with the order of stability C ≥ A2 ≥ A1. In fact, for the C site, the position of Li is found to be slightly displaced off-center by 0.4 Å along the b axis (e.g., fractional coordinates (0.0, 0.6, 0.0)) with Li−O distances of 2.12 Å (×2) and 2.71 Å (×2). Our results are in good agreement with preliminary neutron diffraction studies that indicate that Li occupies an off-center C site in bulk Li_xTiO_2−B for $x \leq 0.25$.[42] Interestingly, an off-center position for inserted Li ions has also been calculated in the case of rutile TiO_2.[15]

The Bader charge analysis indicates a very small change in the electron configuration about Ti atoms, which suggests that the electrons are not localized on a single Ti atom upon lithium insertion. It is also interesting to note that the constant-volume calculations show very similar quantitative results indicating that, for low lithium content, the degree of lattice perturbation is not significant.

A relatively low energy was also found for the A2 5-fold coordinated site. Recently reported DFT simulations of Panduwinata and Gale[12] find that lithium is bound most favorably at a position close to the titania octahedral layer (and similar to our A2 labeled site). The similar energies for these Li insertion sites suggest that for higher lithium content ($x > 0.25$), the intercalated Li could sit on more than one position in the bulk structure. However, we recognize that for such concentrations there may be structural issues related to possible two-phase behavior, which needs to be fully characterized.

Table 3. Calculated Cell Voltages for Low Lithium Content in Li_xTiO_2−B

Li content (x)	voltage (V)
0.031	1.64
0.0625	1.41
0.125	1.29

The calculated voltage as a function of lithium content (Li_xTiO_2−B) has been compared to available experimental data for the bulk phase,[43,44] which has a lower charge and discharge separation compared to nanowires and nanotubes.[45] The voltage is usually measured to be ∼1.5 V vs Li^+ for the different nanostructures[4,44] (when $x = 0.5$). Our resulting data, presented in Table 3, indicate a calculated voltage range of about 1.29−1.64 V for low lithium content ($x < 0.125$). Although this covers a narrow composition range, these calculations are compatible with measured values. Electrochemical studies[44] show sloping voltage profiles for Li_x-TiO_2−B with cell voltage ranges of 1.75−2.0 V for low x (<0.125) on the discharge profile. As with previous GGA studies, the quantitative discrepancy is consistent with the systematic under-prediction of the cell potential in transition metal oxides.[20,37,46] We recognize that the possible sources of DFT error are likely to be attributed to the overbinding of lithium metal and problems with the dispersion term. In any case, our calculated trend in cell voltages as a function of Li content is in accord with experiment.

3.2. Li Diffusion Pathway. Examination of the intrinsic Li ion mobility in TiO_2−B is of vital interest when considering its use as an anode material in lithium batteries. Simulation methods can greatly enhance our understanding of ion diffusion pathways by evaluating the activation energies for various possible mechanisms at the atomic level.

Three main Li conduction paths were considered within the TiO_2−B structure for the low-concentration regime involving conventional hopping of lithium ions between neighboring C site positions (illustrated in Figure 3). These were assigned to path i, migration in the [100] direction, which requires the Li ion to follow a zigzag path within the (001) plane through the A2 site; path ii, migration between adjacent C sites along the [010] direction (parallel to the b-axis channel); and path iii, migration between the b-axis channels through the A1 site along the [001] direction (and parallel to the c axis).

Energy profiles for these mechanisms were mapped out by calculating the energy of the migrating Li ion along the diffusion path, in which full relaxation of the host lattice

(42) Armstrong, A. R., Bruce P. G. **2009**, personal communication.
(43) Inaba, M.; Oba, Y.; Niina, F.; Murota, Y.; Ogino, Y.; Tasaka, A.; Hirota, K. *J. Power Sources* **2009**, *189*, 580.
(44) Armstrong, A. R.; Armstrong, G.; Canales, J.; Bruce, P. G. *Angew. Chem., Int. Ed.* **2004**, *43*, 2286.
(45) Armstrong, G.; Armstrong, A. R.; Canales, J.; Bruce, P. G. *Chem. Commun.* **2005**, 2454.
(46) Reed, J.; Ceder, G. *Electrochem. Solid-State Lett.* **2002**, *5*, A145.

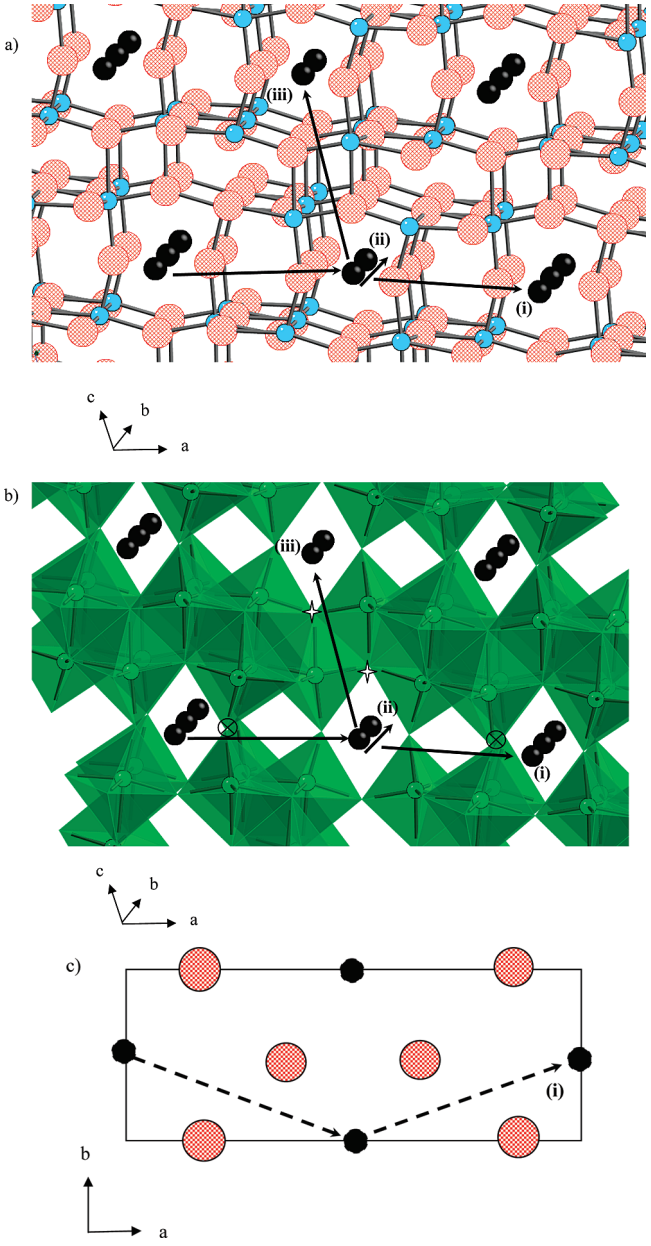

Figure 3. Lithium diffusion paths between C sites (black spheres). (a) Ball-and-stick representation in which large red spheres are oxygen atoms and small blue spheres are Ti atoms; (b) polyhedra representation with TiO_6 octahedra in green; A1 and A2 sites are indicated as stars and crosses, respectively; (c) 2D schematic of path (i).

was allowed for the constant-pressure calculations. In this way the position of highest potential energy (i.e., the "barrier" configuration) was identified from which the migration energy was derived. DFT methods have been used successfully in previous studies on lithium transport in complex oxides,[18] in which the calculations employ the nudged elastic band method and are performed at constant volume. Our resulting energy profiles and migration energies for the three Li diffusion paths in TiO_2−B are given in Figure 4 and Table 4, respectively.

Examination of the results reveals a low energy Li diffusion path (~0.3 eV) along the *b*-axis channel in the [010] direction (path (ii) in Figure 3). We also find a low migration energy (~0.5 eV) along the [001] direction (path (iii)). In contrast, path (i) in the [100] direction has an

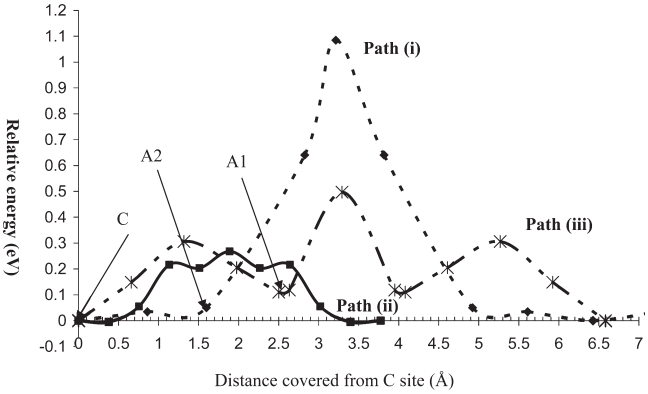

Figure 4. Calculated energy profiles for the three lithium diffusion paths in TiO_2−B, showing the lowest energy barrier for path (ii).

Table 4. Li Migration Paths between C Sites and Calculated Activation Energies in $Li_{0.125}TiO_2$−B

migration path	Li−Li[a] separation (Å)	barrier position	E_a (eV) constant volume	E_a (eV) constant pressure
(i) [100] zigzag	6.43	0.25 0.25 0.00	1.07	0.94
(ii) [010] linear	3.77	0.00 0.00 0.00	0.27	0.29
(iii) [001] linear	6.58	0.00 0.50 0.50	0.50	0.54

[a] Between two C sites shown in Figure 3

unfavorable energy barrier (~1 eV), which suggests that this path makes no significant contribution to Li motion in TiO_2−B. Indeed, the high energy at the barrier position (shown in Figure 4) also indicates that Li insertion sites or a diffusion path along the narrow "channel" parallel to the *b*-axis are unfavorable and, moreover, would not involve the low energy C site. Overall, these results indicate high, albeit anisotropic, Li ion mobility in the TiO_2−B structure. Our results therefore support the assumption often made in experiments that the larger *b*-axis channel is the favored pathway for facile Li diffusion.

Here, it is also interesting to note that the mean Li−Ti separation at the insertion and barrier positions shows a degree of correlation with the calculated energetics and order of stability; the Li insertion and barrier sites with lowest energy have the longest mean Li−Ti separations. Hence, one of the important factors influencing Li insertion and diffusion is the reduction of the electrostatic Li−Ti repulsion.

Although there are limited lithium ion conductivity data on bulk TiO_2−B for direct comparison, our calculated migration energies are consistent with experimental and theoretical activation energies (≤0.5 eV) for related TiO_2 materials.[47−50] Recently reported DFT simulations of Panduwinata and Gale[12] find that Li first needs to migrate from its low-energy position (close to our A2 site)

(47) Koudriachova, M. V.; Harrison, N. M.; de Leeuw, S. W. *Phys. Rev. Lett.* **2001**, *86*, 1275.
(48) Wagemaker, M.; Kentgens, A. P. M.; Mulder, F. M. *Nature* **2002**, *418*, 397.
(49) Olson, C. L.; Nelson, J.; Islam, M. S. *J. Phys. Chem. B* **2006**, *110*, 9995.
(50) Wagemaker, M.; Lützenkirchen-Hecht, D.; van Well, A. A.; Frahm, R. *J. Phys. Chem. B* **2004**, *108*, 12456.

to the center of the *b*-axis channel and then diffuse with a calculated activation energy of 27 kJ/mol (0.28 eV); the latter value is very similar to our calculated energy for diffusion along the *b*-axis channel. Wilkening et al.[8] report stimulated echo NMR studies of higher lithium content $Li_{0.3}TiO_2$−B nanowires, and derive an activation energy of 0.48 eV for long-range Li diffusion. For comparison, it is interesting to note that recent DFT studies on olivine-structured $LiFePO_4$ and layered $LiNiO_2$ electrode materials[18,19] find Li migration energies of ∼0.3 eV for these systems.

Finally, we note that our future computational work on Li_xTiO_2−B will address higher Li content materials ($x > 0.25$) and nanostructures of this system in relation to recent experimental studies.[4,43,51,52]

4. Conclusion

Computational studies based on DFT methods have advanced our understanding, at the atomic level, of lithium insertion sites and diffusion paths in the TiO_2−B lithium battery material, which are relevant to optimizing its electrochemical behavior. These results are also significant in relation to the lithium intercalation properties of TiO_2−B nanotube and nanowire structures. The following main points emerge from our study:

(1) Our simulation model shows good reproduction of the observed crystal structure of TiO_2−B; this structure has a lower packing density than the rutile, anatase and brookite polymorphs of titania. The calculated cell voltage range (1.29−1.64 V) for very low lithium content (x) is compatible with electrochemical measurements on bulk Li_xTiO_2−B.

(2) The most favorable lithium insertion site at low concentration ($x \leq 0.125$ for Li_xTiO_2−B) is found to be the square planar site (termed the C site) with a slightly off-center position in the *b*-axis channel. A relatively low energy was also found for the A2 5-fold coordinated site. For higher lithium content ($x > 0.25$ in Li_xTiO_2−B), the intercalated Li is likely to occupy additional positions to the C site.

(3) The results reveal a low energy (∼ 0.3 eV) pathway for Li ion diffusion along the *b*-axis channel in the [010] direction indicating high Li ion mobility. We also find a low migration energy (∼0.5 eV) along the [001] direction. It is apparent that the TiO_2−B material has adequate intrinsic Li mobility for use as an anode in rechargeable lithium batteries. In view of these two low-energy barrier mechanisms, we suggest that anisotropic transport behavior is expected in TiO_2−B single crystals.

Acknowledgment. We acknowledge the EPSRC for funding as a part of the Supergen Energy Storage Consortium (Grant EP/D031672/1). The computer facilities used are Mott2 (EPSRC Grant GR/S84415/01) and HECToR within the Materials Chemistry Consortium (Grant EP/F067496/1). We also thank P. G. Bruce, Y. Andreev, and A. R. Armstrong at St. Andrews University, U.K., for useful discussions.

Supporting Information Available: Comparison of experimental and calculated unit cell volumes for four TiO_2 structures, the density of states (DOS), the optimized Li_xTiO_2−B (x = 0.031, 0.0625, 0.125) structures, and information on the insertion voltage calculation (PDF). This material is available free of charge via the Internet at http://pubs.acs.org.

(51) Beuvier, T.; Richard-Plouet, M.; Brohan, L. *J. Phys. Chem. C* **2009**, *113*, 13703. Prochazka, J; Kavan, L; Zukalova, M.; Frank, O.; Kalbac, M.; Zukal, A.; Klementova, M.; Carbone, D.; Graetzel, M. *Chem. Mater.* **2009**, *21*, 1457.

(52) Yamamoto, K.; Tomita, K.; Fujita, K.; Kobayashi, M.; Petrykin, V.; Kakihana, M. *J. Cryst. Growth* **2009**, *311*, 619. Li, Q. J.; Zhang, J. W.; Liu, B. B.; Li, M.; Liu, R.; Li, X. L.; Ma, H. L.; Yu, S. D.; Wang, L.; Zou, Y. G.; Li, Z. P.; Zou, B.; Cui, T.; Zou, G. T. *Inorg. Chem.* **2008**, *47*, 9870.